Eur. Phys. J. D **6**, 49–55 (1999)

THE EUROPEAN PHYSICAL JOURNAL D

EDP Sciences

Laser control of intramolecular hydrogen transfer reactions: A real-time path integral approach

O. Kühn[a]

Fachbereich Chemie, WE 3, Freie Universität Berlin, Takustr. 3, 14195 Berlin, Germany

Received: 15 September 1998 / Received in final form: 7 December 1998

Abstract. Different pulse shapes realizing photo isomerization via laser driven tunnelling or vibrational transitions are studied here. Particular attention is paid to the investigation of their robustness with respect to the influence of dissipative processes introduced by the interaction with an environment. An iterative scheme for propagation of the reduced density matrix in the path integral representation is used to take into account arbitrary system-environment coupling strengths as well as the effect of non-Markovian dynamics.

PACS. 31.70.Hq Time-dependent phenomena: excitation and relaxation processes, and reaction rates – 82.40.Js Fast and ultrafast reactions – 82.30.Qt Isomerization and rearrangement

1 Introduction

The possibility to influence the reaction pathway and consequently the reaction yield by means of laser fields has attracted considerable attention recently (for reviews see, *e.g.*, Refs. [1–3]). In particular laser driven isomerization has been on focus in this respect, not at least because of its possible application for switches in molecular electronics devices [4]. Especially, isomerization reactions accompanying intramolecular hydrogen transfer (HT) are of outstanding importance in many chemical and biological processes. (For recent reviews, see [5].) Besides more traditional aspects, HT isomerization reactions can take place on very short time scales making them relevant for femtochemistry studies (see, *e.g.* [6]).

HT in the electronic ground state is typically characterised by a reaction surface showing two minima corresponding to the reactant and the product species which are separated by a reaction barrier. Starting with this system prepared in the reactant state laser induced switching can be realized straightforwardly using a two-pulse pump-dump scheme as outlined, *e.g.*, in [7] and applied to HT in [8]. In contrast to the pump-dump approach where the reaction is driven *over* the barrier, a tunnelling scheme has been proposed from optimal control theory [9]. Here the reaction is driven *through* the barrier, *i.e.* this approach will be appropriate for systems having a rather low barrier. In short, starting with a wave packet localised in the reactant well a constant field is switched-on in a way that would lead to perfectly delocalized tunnelling states in the detuned potential. Choosing the switching time in the range of a few hundred femtoseconds a coherent superposition of these eigenstates of the molecule plus field Hamiltonian is created whose dynamics during the following constant field plateau phase results in tunnelling between reactant and product potential minima. If the field is switched off after about the tunnelling time the wave packet is stabilised in the product well. The main advantages compared to the pump-dump scheme are: first, this approach does not require the rather high field intensities necessary for above barrier driving, and second, there is quite some flexibility concerning the exact form of the laser pulse as discussed in [9]. Since the tunnelling time is dictated by the shape and in particular the height of the barrier this mechanism does not allow for ultrafast switching as soon as the latter increases. In reference [10] it was shown that in this case a two pulse sequence is more appropriate. First, a pump-pulse prepares a vibrationally excited state in the reactant potential well. This state should be chosen such that there is some nearly degenerate state available on the product side. Starting from this excited state a tunnel pulse is then used to transfer the wave packet to the product well.

The pump-dump as well as the tunnelling scheme discussed so far included only a few (two in Ref. [8] and one in Refs. [9,10]) degrees of freedom. If one wishes to abandon such a reduced description and to include the interaction of these HT coordinates with other intramolecular degrees of freedom as well as with a surrounding medium advantage can be taken of density matrix theory [11]. (For an application of density matrix theory to HT see also [12, 13].) In reference [10] it was shown how multilevel Redfield theory [14] can be applied to study the robustness of tunnelling control schemes with respect to energy and phase relaxation processes. This approach of course implies Markovian dynamics as well as a coupling between the HT coordinate and the bath which is rather weak. Further, a straightforward application of Redfield theory

[a] e-mail: ok@chemie.fu-berlin.de

usually neglects the influence of the field on the relaxation rates. For a monochromatic field the latter restriction can be avoided, *e.g.* by using a representation of the reduced density matrix (RDM) in terms of Floquet states [15]. (For a review see also [16].) One alternative to the weak coupling treatment of the system-environment interaction has been given in reference [17] where Franck-Condon weighted tunnel coupling matrix elements obtained after canonical transformation of the total Hamiltonian have been used as a small parameter. Another alternative which includes arbitrary large system-environment coupling within a non-Markovian description of the system dynamics is given by the real-time path integral approach (see, *e.g.*, [16,18]). It was only recently that efficient numerical schemes were developed for propagating the density matrix via path integrals [19–24]. Among the various applications have been, *e.g.*, the study of the real-time dynamics in multi-mode vibronic coupling systems [22], of the resonant electron-molecule scattering [23], and of curve-crossing problems [24,25].

In cases where the energy spectrum of the double minimum potential allows for a separation of the lowest tunnel doublet from higher excited states, the dissipative HT dynamics can be described by the spin-boson model [18]. The dynamics in this two-level model system driven by shaped, pulsed or pure monochromatic laser light has been studied extensively during the last years. (For a recent review see [16].) In particular, it was shown that monochromatic light can lead to coherent destruction of tunnelling, *i.e.* preserve an initially localised non-eigenstate of the isolated system [26]. On the other hand, an initially delocalized state can become localised by means of a suitable chosen field [27]. The influence of dissipation on the population transfer under monochromatic driving was studied in detail in references [15,17,28,29], for instance.

In the present contribution we investigate laser pulses of different shapes which are capable of driving HT at high yield in the absence of dissipation. Emphasis is paid to the investigation of their ability to compete with relaxation processes in the presence of dissipation. The latter is described using a real-time path integral representation of the RDM. The remaining text is organised as follows: We first introduce the model system in Section 2. The potential for the reaction coordinate is chosen to mimic hydrogen transfer in thioacetylacetone (TAA) for which high-level *ab initio* calculations have been performed [30]. In Section 3 a brief outline of the numerical procedure for propagation of the RDM using the iterative tensor propagation scheme developed by N. Makri and co-workers is given [19,20,31]. The numerical simulations are discussed in Section 4 and the paper is summarised in Section 5.

2 The model

When investigating controlled photo isomerization it is desirable to consider intramolecular HT in molecules having energetically non-equivalent reactant and product configurations. This allows for a clear distinction between initial and final states when following the reaction, *e.g.*, using time resolved pump-probe spectroscopy. While in references [8–10] general non-symmetrical substituted malonaldehyde has been taken as a reference system the present simulations will be done for a specific molecule, TAA. A detailed account for the quantum chemical calculations will be given in reference [30]. In short, MP2 calculations using a $6-31+\mathrm{G(d,p)}$ basis set have been performed to locate the stationary points as well as the transition state configuration on the potential energy surface. Using these data the empirical one dimensional potential function

$$V(x) = \frac{1}{2}\Big[V_{\rm osc}^{(1)}(x) + V_{\rm osc}^{(2)}(x) - \sqrt{(V_{\rm osc}^{(1)}(x) + V_{\rm osc}^{(2)})^2 + 4K^2(x)}\Big] \qquad (1)$$

was fitted to reproduce the energetics at the calculated points as well as the different local vibrations on the reactant (O–H) and product (S–H) side. In equation (1), $V_{\rm osc}^{(i)}(x) = k_i(x-x_{0,i})^2/2+\Delta_i$, are local diabatic potentials which are coupled via the function $K(x) = k_c e^{-(x-x_c)^2}$. The adiabatic potential, $V(x)$, is shown in Figure 1 together with the wave functions of the two lowest eigenstates which are rather localised and energetically below the reaction barrier (for parameters see figure caption). The dipole moment was fitted to a linear function, $d(x)$, interpolating between the values 4.27 D and 3.75 D obtained for the two stationary points [30]. Taking this information together we are able to write down the Hamiltonian of the reactive system coupled to the laser

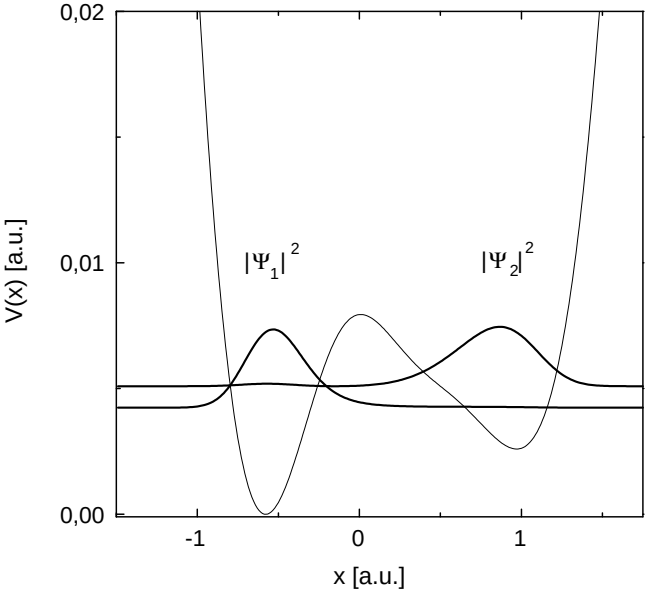

Fig. 1. One dimensional potential curve, $V(x)$ for isomerization in TAA. The parameters entering equation (1) are: k_1=5.95 mD/A k_2 =4.31 mD/A, $x_{0,1} = -0.38$ A , $x_{0,2} = 0.64$A , Δ_1=0, Δ_2=0.0975 eV, $k_c = 4.24$ eV, and $x_c = 0.152$ A. The barrier height is 0.214 eV and the asymmetry is 0.07 eV. For details see reference [30]. The two lowest eigenfunctions are shown with a vertical offset corresponding to the respective eigenenergies.

field:

$$H_{\rm s}(t) = \frac{p^2}{2m} + V(x) - d(x)\mathcal{E}(t) \; . \tag{2}$$

For simplicity we will assume that the field is always directed along the systems dipole moment. In order to account for the environmental degrees of freedom we supplement equation (2) with a coupling term which reads

$$H_{\rm s-e} = \sum_j \frac{P_j}{2M_j} + \frac{1}{2}M_j\Omega_j^2\left(Q_j - \frac{f(x)}{M_j\Omega_j^2}\right)^2 \; , \tag{3}$$

with M_j and Ω_j being the mass and the frequency of the jth oscillator, respectively. $\{Q_j\}$ and $\{P_j\}$ are the oscillator coordinates and conjugate momenta. For the coupling function we will use $f(x) = c_j x$ for simplicity. Equations (2) and (3) have the form of the generic system-environment Hamiltonian which has been extensively used to study condensed phase dynamics. (See, *e.g.*, [16,18,19, 21].) Within this system-bath model the influence of the bath is characterised by its spectral density, $\mathcal{J}(\omega)$, which reads

$$\mathcal{J}(\omega) = \frac{\pi}{2}\sum_j \frac{c_j^2}{M_j\Omega_j}\delta(\omega - \Omega_j) \; . \tag{4}$$

In the numerical simulations presented below we have chosen the empirical form

$$\mathcal{J}(\omega) = \frac{\pi}{2}\xi\omega e^{-|\omega|/\omega_{\rm c}} \; . \tag{5}$$

This Ohmic type spectral density is commonly used [19, 21] as being typical for a condensed phase environment characterised by some frequency $\omega_{\rm c}$ limiting the range of modes which can couple to the system. For the present application we used $\omega_{\rm c} = 500$ cm^{-1} in order to model particularly the influence of low frequency vibrations of the molecular scaffold on the HT dynamics. The coupling strength is given by the dimensionless Kondo parameter ξ.

3 Density matrix propagation

The time evolution of the HT system under the influence of the dissipative environment can be obtained from the RDM. Given the total density operator, $\rho_{\rm tot}$, at some time t_0 the RDM, $\rho(t_N)$, at time t_N is obtained from

$$\begin{aligned}\rho(x_N^+, x_N^-; t_N) = {\rm Tr}_{\rm e}[\langle x_N^+|U(t_N,t_0)\rho_{\rm tot} \\ \times U^\dagger(t_N,t_0)|x_N^-\rangle] \, ,\end{aligned} \tag{6}$$

where we used $|x_N^\pm\rangle$ to label the coordinate state vectors and ${\rm Tr}_{\rm e}$ denotes the trace with respect to the environmental degrees of freedom. The practical evaluation of equation (6) requires discretization of the time axis by introducing N segments of length $\Delta t = (t - t_0)/N$, *i.e.* $t_i = t_0 + i\Delta t$ $(i = 0, \ldots, N)$. The composition law for the evolution operator then gives $U(t_N, t_0) = U(t_N, t_{N-1}) \ldots U(t_1, t_0)$, $(t = t_N)$. For the short time propagator, $U(t + \Delta t, t)$, a symmetric splitting is performed, *i.e.* [19]

$$\begin{aligned}U(t + \Delta t, t) = U_{\rm s-e}(t + \Delta t/2, t)U_{\rm s}(t + \Delta t, t) \\ \times U_{\rm s-e}(t + \Delta t/2, t) \, ,\end{aligned} \tag{7}$$

where $U_{\rm s}(t', t)$ and $U_{\rm s-e}(t', t)$ denote the time evolution operator with respect to the Hamiltonian (2) and (3), respectively. As is well known, the error made when using equation (7) is proportional to the system-environmental coupling strength [20]. Supplementing this splitting by the initial condition $\rho_{\rm tot} = \rho(t_0)\rho_{\rm e}$, where $\rho_{\rm e}$ is the equilibrium statistical operator for the environment, one obtains for the RDM [19]

$$\begin{aligned}\rho(x_N^+, x_N^-; t_N) = \int {\rm d}x_0^\pm \ldots dx_{N-1}^\pm \rho(x_0^+, x_0^-; t_0) \\ \times I(x_0^\pm, \ldots, x_N^\pm; \Delta t) \\ \times \prod_{j=1,N} K(x_j^\pm, x_{j-1}^\pm) \, .\end{aligned} \tag{8}$$

Here

$$\begin{aligned}K(x_j^\pm, x_{j-1}^\pm) = \langle x_j^+|U_{\rm s}(t_j, t_{j-1})|x_{j-1}^+\rangle \\ \times \langle x_{j-1}^-|U^\dagger(t_{j-1}, t_j)|x_j^-\rangle\end{aligned} \tag{9}$$

is the free system propagator matrix. The effect of the interaction with the environment is contained in the influence functional $I(x_0^\pm, \ldots, x_N^\pm; \Delta t)$ [32]. While equation (8) is exact and includes the memory effects which are neglected in the Redfield treatment, numerical methods for investigating the long time dynamics using this path integral expression have been developed only recently [19, 33,31]. In the following we will use the approach put forward by Makri and co-workers (for a recent review, see also Ref. [20] and for the numerical implementation, cf. [31]). which rests on the observation that in condensed phase environments non-local memory effects have only a finite span. This is reflected in the fact that the so-called bath response function

$$\alpha(t) = \frac{1}{\pi}\int_0^\infty {\rm d}\omega\mathcal{J}(\omega)[\coth(\omega/2k_{\rm B}T)\cos(\omega t) - i\sin(\omega t)] \tag{10}$$

decays on the time scale of the memory time which reads in units of the time step $\tau_{\rm mem} = k_{\rm mem}\Delta t$. This allows one to develop an iterative scheme for propagating an augmented density matrix which can be mapped onto a vector of length $N_{\rm bound}^{2k_{\rm mem}}$, where $N_{\rm bound}$ is the number of bound states of the relevant system (for details see [31]). The actual value of $\tau_{\rm mem}$ is dictated by the temperature and the form of the spectral density $\mathcal{J}(\omega)$. For the Ohmic spectral density of equation (5), $\alpha(t)$ decays to zero on a rather short time scale of a few tens of femtoseconds at room temperature.

The actual numerical evaluation of equation (8) has been performed using a system-specific discrete variable representation (DVR) [19,20,31]. In order to accomplish an efficient calculation of the matrix elements of the system propagator we used the time-dependent version of the

DVR as outlined in reference [34]. In short, one starts with generating a dynamical orthogonal set of basis functions, $\{\varphi_n(t)\}$ $(n = 1, \ldots, N_{\mathrm{bound}})$, by application of the system propagator to some initial set $\{\varphi_n(t = 0)\}$,

$$\varphi_n(t) = U_{\mathrm{s}}(t, 0)\varphi_n(0). \tag{11}$$

For the $\{\varphi_n(0)\}$ we have chosen the set of eigenstates of the field-free Hamiltonian, $\{\Psi_n\}$, which were obtained using the Fourier grid method [35]. (Cf. also Fig. 1.) The propagation was then performed by converting equation (11) into a set of coupled first order differential equations which have been solved using an extrapolation method. Next the position operator was represented in this time-dependent basis set and the resulting matrix was diagonalised to obtain the time-dependent DVR states solving

$$x|\chi_\lambda(t)\rangle = x_\lambda(t)|\chi_\lambda(t)\rangle\,. \tag{12}$$

Using these DVR states the matrix elements of the system propagator entering equation (8) can be obtained from [34]

$$\langle\chi_\lambda(t+\Delta_t)|U_{\mathrm{s}}(t+\Delta t, t)|\chi_{\lambda'}(t)\rangle = \sum_{n=1}^{N_{\mathrm{bound}}} C_{\lambda n}(t+\Delta t)C_{n\lambda'}(t)\,. \tag{13}$$

Here $C_{n\lambda}(t) = \langle\varphi_n(t)|\chi_\lambda(t)\rangle$ is coefficient matrix for transformation between the time-dependent basis set $\{\varphi_n(t)\}$ and the DVR basis $\{\chi_\lambda(t)\}$.

The numerical results presented in the following section have been obtained after carefully adjusting the time step, Δt, as well as the memory length, k_m, until convergence with respect to the populations dynamics was reached. Depending on the coupling strength parameter ξ, Δt was about 1 fs and values of k_{mem} up to 10 have been used.

4 Discussion of numerical results

In the following we present the population dynamics for the eigenstates of the field-free isolated molecule, Ψ_n, for three different shapes of the driving field. The respective RDM elements, $\rho_{nn}(t)$, are calculated straightforwardly from equation (8) by using a basis set transformation. The splitting between the two lowest states in the energy spectrum of the field-free isolated molecule (see Fig. 1) is much smaller ($E_2 - E_1 \approx 0.023$ eV) than the energy gap separating them from the higher excited states ($E_3 - E_2 \approx 0.1$ eV). Furthermore, for the driving fields employed subsequently, population of states with quantum numbers $n > 2$ is usually smaller than 0.01. Therefore, it is possible to restrict our model of HT dynamics in TAA to a two-level system coupled to a dissipative environment. For the initial condition we have used $\rho_{nn}(t = 0) = \delta_{n1}$ for simplicity, which corresponds to $\rho_{11}(0) - \rho_{22}(0) = 1$ in the following figures. All calculations have been performed for room temperature. The pulses were chosen in a way to yield an almost complete population inversion between the two states for the isolated system. Since these states

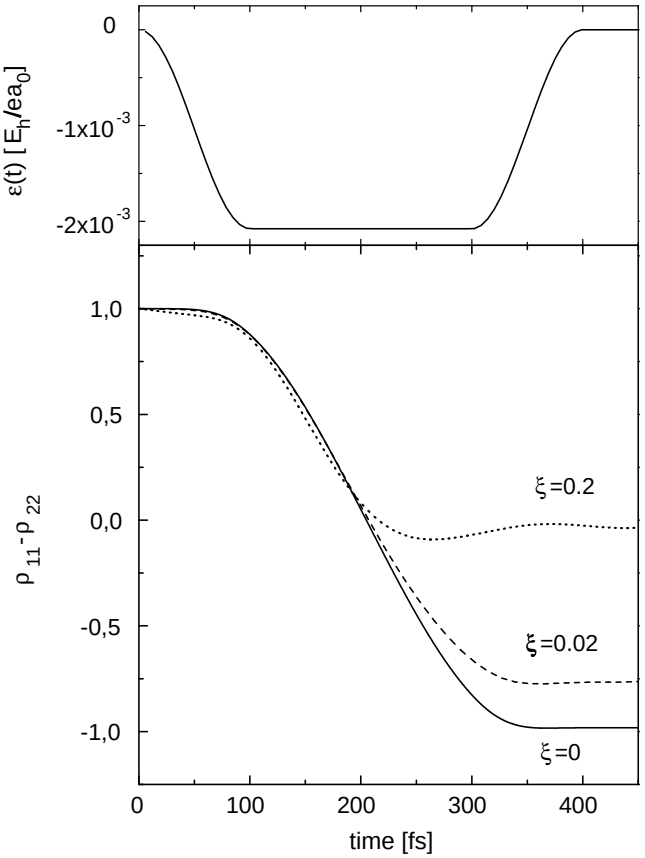

Fig. 2. Driving field (upper panel) and induced population dynamics (lower panel) of the two eigenstates shown in Figure 1 for various values of the system environment coupling parameter ξ. For the field parameters See text.

are rather localised on either the reactant or the product side (see Fig. 1), population switching corresponds to HT.

In Figure 2 we have plotted the population dynamics of our model system using the simple tunnel pulse proposed in reference [9]. The pulse is shown in the upper panel and includes a 100 fs $\sin^2$-type switch-on and switch-off period and a 200 fs constant field plateau period. The plateau field has been determined from the condition $\mathcal{E}_{\mathrm{p}} = (E_1 - E_2)/(d_{11} - d_{22})$ [10], where E_n and d_{nn} are the eigenvalues and dipole matrix elements of the isolated system Hamiltonian.

Since the tunnelling mechanism relies on the dynamics of a coherent superposition of states it is heavily influenced by relaxation processes introduced by the interaction with the environment. This can be seen in Figure 2 where we show the dynamics for three different values of the coupling strength parameter ξ. It is important to remember at this point, that the present approach includes the effect of the field on the relaxation. This implies that as long as the field is switched-on relaxation will drive the system towards an equilibrium with respect to the *instantaneous* molecule plus field Hamiltonian. This equilibrium is not yet established at $t = 300$ fs in Figure 2. If the field is not switched-off the population dynamics shows damped oscillations (not shown).

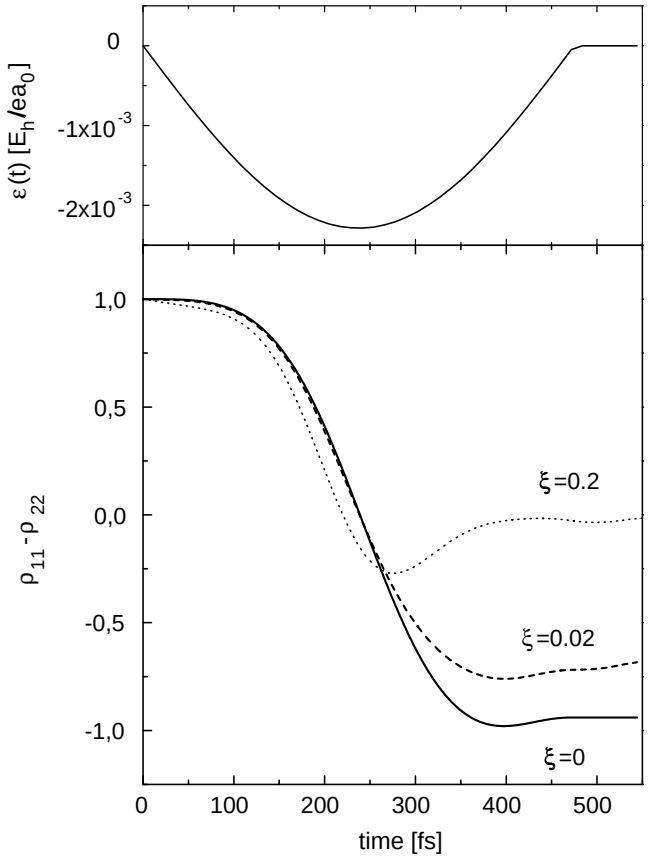

Fig. 3. Same as in Figure 2 but for a half-cycled driving pulse. For the field parameters see text.

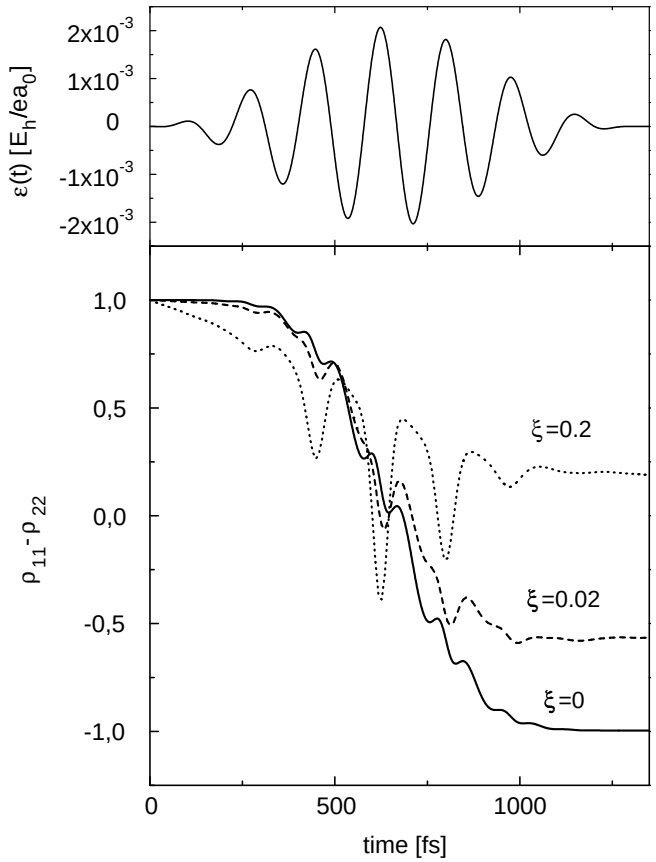

Fig. 4. Same as in Figure 2 but for a $\sin^2$ shaped pulse modulated by some carrier frequency. For the field parameters see text.

In the moment the field is switched-off the system will start to relax towards its field-free equilibrium state. This process takes place on a picosecond time scale for the chosen coupling strengths, partly because $\hbar\omega_c$ is much larger than $E_2 - E_1$. It should be noticed that with the so-called counter term included in the Hamiltonian, the barrier height does not depend on the system-environment coupling strength. However, the shape of the multidimensional potential surface of the total system is modified as can be seen from equation (3) (see, *e.g.*, [36]). Thus the equilibrium populations of the isolated system eigenstates in general will depend on the Kondo parameter. (For an estimate of the effect, see, *e.g.*, [33].)

The pulse form shown in the upper panel of Figure 2 is certainly not easily realized in an actual experiment. Fortunately, there is some flexibility concerning the pulse shape as discussed in [9]. In particular so-called half-cycled pulses can be used to drive HT at comparable high yield. High-power subpicosecond half-cycled pulses, however, have been generated recently by Bucksbaum and coworkers [37]. In Figure 3 we show the population dynamics for driving the reaction with a half-cycled pulse. The maximum switching (about 97 %) has been obtained using a 475 fs sin-shaped pulse having an amplitude which is 1.1 times $\mathcal{E}_p$ (see upper panel of Figure 3). Since the pulse length did not change appreciably, the switching yield in the presence of dissipation is comparable to the one obtained in Figure 2. A close inspection of Figures 1 and 2 reveals only a slight modification of the population dynamics.

As a third example of a laser field suitable for driving isomerization reactions we consider the simple form $\mathcal{E}(t) = E_0 \sin^2(\pi t/\tau)\cos(\omega_p t)$ used, *e.g.* in references [7, 8] in the context of pump-dump control. The possibility of driven HT by such pulses has been indicated by optimal control theory [38]. Choosing $E_0 = \mathcal{E}_p$ and $\hbar\omega_p = (E_2 - E_1)$ requires a pulse duration of $\tau = 1300$ fs in order to achieve close to 100 % switching probability for the isolated case. The resulting field is shown in the upper panel of Figure 4. In the lower panel of Figure 4 we plotted the corresponding dynamics of the occupation probabilities for various strength of the system-environment coupling. Surprisingly the effect of this coupling is not as disastrous for the switching yield as one might have anticipated for a pulse more than twice as long as in Figures 2 and 3. For the strongest coupling used we still have a non-equilibrium population of the states at the moment the field is smoothly switched-off. Again the reason can be found in the fact that the relaxation takes into account the influence of the driving field. The situation is, however, much more complicated than in the previous examples where the population switched smoothly on the time scale of the pulse envelope. Superimposing an oscillating

component on the pulse envelope already yields oscillations in the dissipation free population dynamics. In this case the field "shakes" the potential $V(x)$ back and forth; the net effect being a population inversion at the end of the pulse. It should be noted that in the present case of a resonantly driven two-level system the area theorem applies, *i.e.* the pulse shown in Figure 4 is a so-called π-pulse [39]. Turning on the interaction with the environment, laser driving and relaxation according to the instantaneous potential compete what gives rise to the pronounced population oscillations. Here the net effect is a population switching whose efficiency depends on the time scales of the driving field (τ and $\omega_{\rm p}$) and of the relaxation (ξ).

Comparing the population difference obtained by the different pulses for the same coupling strength, ξ, the shorter tunnelling pulses are of course more efficient. For a fixed laser frequency, $\omega_{\rm p}$, the only way to increase the switching yield of the $\sin^2$ pulse for a chosen ξ would be a decrease of the pulse duration at the expense of an increased field amplitude. Such a pulse, however, would be spectrally broader and, therefore, might excite higher vibrational levels. This can be expected to deteriorate the selectivity of the HT.

5 Conclusions

In summary a non-Markovian, non-perturbative density matrix description of laser driven intramolecular hydrogen transfer reactions has been presented. The parameters where chosen to model thioacetylacetone for which high level *ab initio* data are available [30]. Different pulse shapes have been judged with respect to their ability to compete with dissipation processes. The pulse shape flexibility of the tunnelling scheme for reaction control proposed in reference [9] has been shown to persist in the dissipative regime. On the other hand, shaped laser pulses inducing a vibrational transition between states localised on different sides of the reaction barrier are more strongly affected by dissipation processes. State selectivity as well as the desire for low pulse intensities requires that they are considerably longer than the tunnel pulses. However, both control schemes for dissipative hydrogen transfer can be considered superior to the above barrier pump-dump method since (i) the pump-dump method requires higher field strength and longer pulses and (ii) above barrier transfer involves higher excited vibrational states for which population relaxation is usually fast.

The robustness of the tunnelling scheme with respect to the interaction with an environment relies not only on the time scale but also on the fact that the maximum of the spectral density is well above the level splitting of the system states. The empirical parameter $\omega_{\rm c}$ had been chosen to model those low frequency vibrational modes of TAA which can be expected to have the strongest influence on the hydrogen's motion (*e.g.*, by varying the O–S distance). However, since the form of the spectral density is rather crucial for the dynamics, simulations leading to experimental realisation of controlled hydrogen transfer in a specific molecule will require more microscopic input. Future work will be focussed on this issue for which the theoretical background has been provided, *e.g.*, by Miller and co-workers [40].

I gratefully acknowledge stimulating discussions on different aspects of laser control with N. Došlić, K. Sundermann, J. Manz (Freie Universität Berlin), and J. Shao (University of Illinois). This work was financially supported by the Deutsche Forschungsgemeinschaft (project Ku952/2-1).

References

1. *Femtosecond Chemistry*, edited by J. Manz and L. Wöste (VCH, Weinheim, 1995).
2. S.A. Rice, Adv. Chem. Phys. **101**, (1997) 213.
3. J. Manz in *Femtochemistry and Femtobiology: Ultrafast Reaction Dynamics at Atomic-Scale Resolution*, edited by V. Sundström, (Imperial College Press, London, 1997) p. 80.
4. R.I. Cukier, M. Morillo in *Molecular Electronics*, edited by J. Jortner and M. Ratner, (Blackwell Science, 1997) p. 119.
5. *Hydrogen Transfer: Experiment and Theory*, edited by H.-H. Limbach, J. Manz, Ber. Bunsenges. Phys. Chem. **102**, (1998) (special issue).
6. T. Elsaesser in *Femtochemistry*, edited by J. Manz and L. Wöste, (VCH, Weinheim, 1995) p. 563.
7. M.V. Korolkov, J. Manz, G.K. Paramonov, J. Chem. Phys. **105**, 10874 (1996).
8. N. Došlić, O. Kühn, J. Manz, Ber. Bunsenges. Phys. Chem. **102**, 292 (1998).
9. N. Došlić, O.Kühn, J. Manz, K. Sundermann, J. Phys. Chem. A **102**, 9645 (1998).
10. H. Naundorf, K. Sundermann, O. Kühn, Chem. Phys. **240**, 163 (1999).
11. K. Blum, *Density Matrix Theory and Applications* (Plenum Press, New York, 1981).
12. O. Brackhagen, O. Kühn, J. Manz, V. May, R. Meyer, J. Chem. Phys. **100**, 9007 (1994).
13. C. Scheurer, P. Saalfrank, J. Chem. Phys. **104**, 2869 (1996).
14. A.G. Redfield, Adv. Magn. Res. **1**, 1 (1965).
15. T. Dittrich, B. Oelschlägel, P. Hänggi, Europhys. Lett. **22**, 5 (1993).
16. M. Grifoni, P. Hänggi, Phys. Rep. **304**, 229 (1998).
17. M. Morillo, R.I. Cukier, Phys. Rev. B **54**, 13962 (1996).
18. U. Weiss, Quantum Dissipative Systems, Series in Modern Condensed Matter Physics, Vol. 2 (World Scientific, Singapore, 1993).
19. N. Makri, J. Math. Phys. **36**, 2430 (1995).
20. N. Makri, J. Phys. Chem. A **102**, 4414 (1998).
21. C.H. Mak, R. Egger, Adv. Chem. Phys. **XCIII**, 39 (1996).
22. S. Krempl, M. Winterstetter, H. Plöhn, W. Domcke, J. Chem. Phys. **100**, 926 (1994).
23. M. Winterstetter, W. Domcke, Phys. Rev. A **47**, 2838 (1993).
24. R.D. Coalson, J. Phys. Chem. **100**, 7896 (1996).
25. D.E. Makarov, N. Makri, Phys. Rev. A **48**, 3626 (1993).
26. F. Grossmann, T. Dittrich, P. Jung, P. Hänggi, Phys. Rev. Lett. **67**, 516 (1991).

27. R. Bavli, H. Metiu, Phys. Rev. Lett. **69**, 1986 (1992).
28. N. Makri, L. Wei, Phys. Rev. E **55**, 2475 (1997).
29. G. Taft, N. Makri, J. Phys. B: At. Mol. Opt. Phys. **31**, 209 (1998).
30. N. Došlić, K. Sundermann, L. Gonzalez, O. Mo, J. Giraud-Girard, O. Kühn, Phys. Chem. Chem. Phys. (in press).
31. E. Sim, N. Makri Comp. Phys. Commun. **99**, 335 (1997).
32. R.P. Feynman, F.L. Vernon, Ann. Phys. **24**, 118 (1963).
33. N. Makri, D.E. Makarov, J. Chem. Phys. **102**, 4600 (1995).
34. E. Sim, N. Makri, J. Chem. Phys. **102**, 5616 (1995).
35. C.C. Marston, G.B. Balint-Kurti, J. Chem. Phys. **91**, 3571 (1989).
36. N. Makri, W.H. Miller, J. Chem. Phys. **86**, 1451 (1987).
37. D. You, R.R. Jones, P.H. Bucksbaum, D.R. Dykaar, Opt. Lett. **18**, 290 (1993).
38. K. Sundermann, N. Došlić, private communication.
39. L. Allen, J.H. Eberly, *Optical Resonance and Two-Level Atoms*, (Dover, New York, 1987).
40. B.A. Ruf, W.H. Miller, J. Chem. Soc., Faraday Trans. 2, **84**, 1532 (1988).